Proceedings World Geothermal Congress 2000
Kyushu - Tohoku, Japan, May 28 - June 10, 2000

AN INVESTIGATION OF BOILING PROCESSES IN HYDROTHERMAL ERUPTIONS

Thomasin Smith and Robert McKibbin
Institute of Fundamental Sciences, Massey University, Private Bag 11 222, Palmerston North, New Zealand

Keywords: geothermal systems, boiling in porous media, hydrothermal eruption, mathematical modelling

ABSTRACT

Development of mathematical models for hydrothermal eruptions depends crucially on understanding transient boiling processes in porous media. In this paper we report on work in progress, where observations from laboratory experiments are compared with results from numerical simulations using a mathematical model based on conservation laws. While qualitative results are similar, more investigation is needed. Differences in experimental and simulation configurations need to be resolved in order to gain quantitative agreement.

1. INTRODUCTION

Hydrothermal eruptions are violent events. They eject a mixture of water, steam and rock particles without warning. Though rare temporally, many have occurred in geothermal fields around the world.

A summary of work that has been done on the modelling of hydrothermal eruptions is given in Smith & McKibbin (1997). Information from the works summarised there has been integrated to form the following conceptual model.

1.1 The Conceptual Model

In geothermal fields susceptible to hydrothermal eruptions, liquid water or a two-phase water mixture lies below the surface at boiling-point conditions. This hot fluid is then suddenly exposed to reduced pressure conditions due to some initiation event [see Figure 1(a)]. Suggested initiation events include seismic activity, hydraulic fracturing (Bixley & Browne, 1988), climatological factors (Allis, 1984), and the drainage of glacially-dammed lakes (Muffler *et al*., 1971).

The pressure reduction causes boiling to occur and the fluid to expand. A common misconception is that the fluid lying below the surface boils causing an increase in the pressure and that this pressure build-up eventually causes an 'explosion' which throws material upwards. This is thermodynamically incorrect. The in-situ formation liquid will not boil unless depressurization occurs. The continuation of this boiling relies on escape paths being provided. If escape paths are not provided the fluid will not boil. If escape paths are provided the fluid will move towards regions of lower pressure and will therefore move upwards. The upward fluid velocities provide lift to the rock above, and if this lift is large enough to overcome the weight and cohesive stresses of the rock, then a rock and fluid mix are ejected upwards. Shear forces, or drag, created by the upward movement may also take some of the forming crater wall up along with it. The fluid will continue to flash as it rises and the eruption column is therefore likely to have a greater steam fraction at the top than it does towards the bottom [see Figure 1(b)].

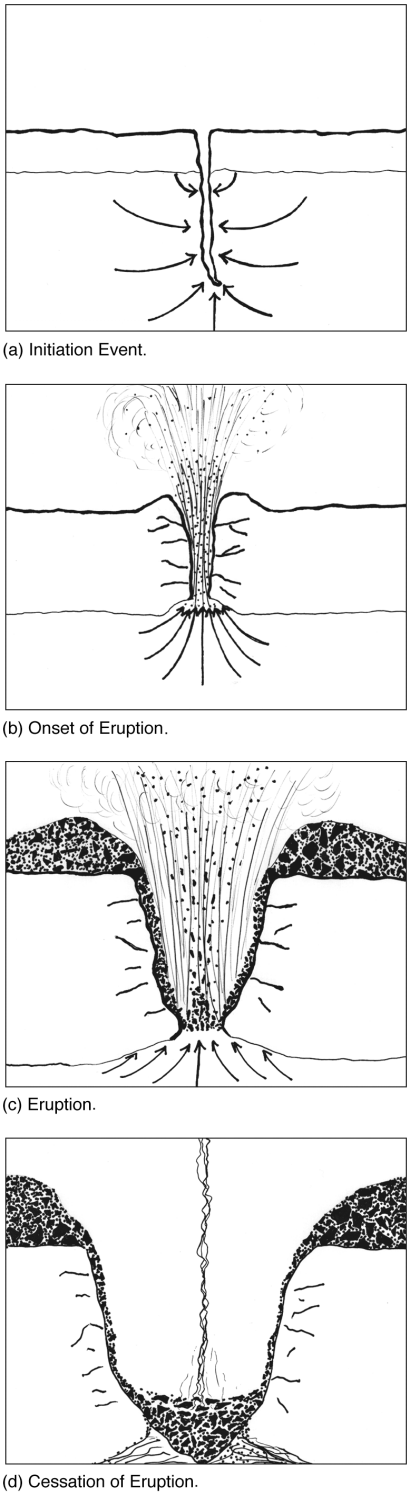

Figure 1. Schematic diagram of the eruptive process.

As fluid and rock are ejected upwards, the depressurisation propagation path progresses downwards, causing the boiling front to continue downwards, prompting more fluid and rock to be ejected. Much of the material falls back into the vent and is re-ejected in the eruptive stream. In general, the finer the debris, the further it is thrown from the vent [see Figure 1(c)].

The continuing advancement of the boiling front is dependent on hot-water recharge or the inflow of heated water to the two-phase conduit. The front will stop progressing if it encounters a region in the rock matrix of negligible permeability.

As the eruption continues, pressure reduction, cooling effects, and gravitational slowing dissipate the energy of the eruption, and the eruption slows and eventually stops. Much of the erupted material falls back into, and is eventually left in, the formed crater. Residual steam continues to rise from the crater floor [see Figure 1(d)].

Due to the release of formation stresses, the walls of the crater formed during the eruption will eventually begin to slump inwards. The loss of significant amounts of material from under the surface may also cause the ground to locally subside.

From this conceptual model it can be noted that the process which drives the hydrothermal eruption is the boiling of water. It is the behaviour of the *boiling front* as it moves through the porous medium that we investigate in the rest of this paper through both numerical and physical experiments.

2. NUMERICAL EXPERIMENT

In modelling hydrothermal eruptions, the principles of conservation of mass, momentum and energy are used to formulate the mathematical problem. A set of non-linear partial differential equations governing transient mass and energy transport may be obtained. Details of these equations are given in Smith & McKibbin (1998).

In this section we look at the simpler case of solving these equations in one horizontal dimension. A one-dimensional "core" of semi-infinite length is initially saturated with liquid water and at some constant pressure throughout. If, as in the case of the hydrothermal eruption, the pressure is then reduced at one end of the porous medium, the pressure reduction will cause boiling to occur and flow to commence. A boiling front will be initiated at the end of the core and will quickly progress through the porous medium (see Figure 2).

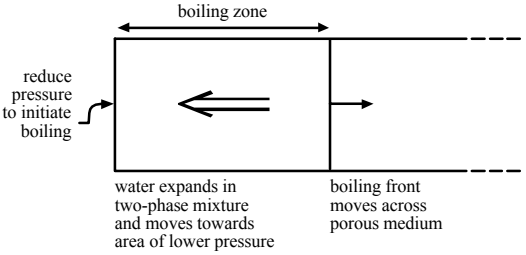

Figure 2. Propogation of boiling front in a porous medium.

We present here two models for this fluid flow. In forming our models, we consider a small representative elementary volume taken from the porous medium which is large enough to contain both some rock and some fluid, but is small enough that the density of the water mixture in the volume is uniform throughout. In our first model, we assume that because of the rapidity of motion, a separable two-phase flow does not have time to develop. Therefore, the fluid is considered to be a homogeneous mixture of liquid and gas. In the second model, this assumption is not made and the water mixture is modelled as two separable phases.

In both models, the conservation of mass and energy equations can be written respectively as follows

$$\frac{\partial A_m}{\partial t} = -\frac{\partial \mathbf{Q}_m}{\partial x} \tag{1}$$

$$\frac{\partial A_e}{\partial t} = -\frac{\partial \mathbf{Q}_e}{\partial x} \tag{2}$$

where A_m and A_e are the fluid mass and energy per unit volume of formation and $\mathbf{Q}_m$ and $\mathbf{Q}_e$ are the mass and energy fluxes per unit area. The time t is taken to be zero at the moment the end of the core is depressurised and the positive distance x is measured from this end of the core.

Expressions for A_m, A_e, $\mathbf{Q}_m$, and $\mathbf{Q}_e$ in terms of matrix and fluid parameters are given in Section 2.1 for the homogeneous mixture flow case and in Section 2.2 for the separable phase flow case. In both cases, Equation (1) states that the time rate of increase of mass inside a representative elementary volume equals the mass flow rate across the surface of the volume, while Equation (2) states that the change in energy inside the volume is equal to the advected energy flow rate across the surface plus the energy gained or lost by conduction.

2.1 Homogeneous Mixture (HM) Flow Model

In the case of the homogeneous mixture model, a single-phase Darcy's Law with parameters that depend on the two-phase fluid mixture is used in describing the mass flow rate per unit area. Under this assumption we have

$$A_m = \phi \rho_f \tag{3}$$

$$A_e = (1-\phi)\rho_r c_r T_{sat} + \phi \rho_f u_f \tag{4}$$

$$\mathbf{Q}_m = k \frac{\rho_f}{\mu_f} \left(-\frac{\partial p}{\partial x} \right) \tag{5}$$

$$\mathbf{Q}_e = h_f \mathbf{Q}_m + K \left(-\frac{\partial T_{sat}}{\partial x} \right) \tag{6}$$

Here the subscript f is used to represent the fluid mixture and the subscript r represents the rock matrix. The rock properties are assumed to be constant and are given as follows: ϕ is the porosity, k is the permeability, c_r is the specific heat, K is the thermal conductivity, and ρ_r is the rock density. The properties of the fluid are: ρ_f is the fluid density, μ_f is the dynamic viscosity, h_f is the specific enthalpy, and u_f is the specific internal energy. $T_{sat}(p)$ is the saturation temperature, the temperature at which water boils for a given pressure p. Alternatively, for a given temperature T, $p_{sat}(T)$ is the

saturation pressure. At such so-called saturated conditions, both liquid water and water vapour may be present in the system. Saturation temperature increases with increasing pressure (see for example any standard set of steam tables).

The density, specific enthalpy and specific energy of the two-phase fluid mixture are given by

$$\rho_f = S\rho_l + (1-S)\rho_g \tag{7}$$

$$h_f = \frac{S\rho_l h_l + (1-S)\rho_g h_g}{S\rho_l + (1-S)\rho_g} \tag{8}$$

$$u_f = Su_l + (1-S)u_g \tag{9}$$

and the mixture dynamic viscosity is chosen to be of the form

$$\mu_f = S\mu_l + (1-S)\mu_g \tag{10}$$

Here S is the liquid saturation (volume fraction of fluid that is liquid) and the subscripts l and g generally refer to the liquid and gas phases.

The fluid is at saturated (boiling) conditions, and standard correlations for thermodynamic properties may be used.

The expressions (3) – (10) are substituted into the conservation of mass and energy equations (1) and (2), to give:

$$A_1 p_t + B_1 S_t = C_1 p_x S_x + D_1 \left(p_x\right)^2 + E_1 p_{xx} \tag{11}$$

$$A_2 p_t + B_2 S_t = C_2 p_x S_x + D_2 \left(p_x\right)^2 + E_2 p_{xx} \tag{12}$$

where the coefficients A_1, A_2, B_1, B_2, C_1, C_2, D_1, D_2, E_1, and E_2 are non-linear functions of pressure and saturation, and the subscripts x and t are used to represent the partial derivatives with respect to x and t respectively.

Equations (11) and (12) may then be reduced to a simpler set of ordinary differential equations by use of the similarity variable $\eta = x/\sqrt{t}$.

$$\frac{1}{2}\eta A_1 p' + \frac{1}{2}\eta B_1 S' = C_1 p' S' + D_1 \left(p'\right)^2 + E_1 p'' \tag{13}$$

$$\frac{1}{2}\eta A_2 p' + \frac{1}{2}\eta B_2 S' = C_2 p' S' + D_2 \left(p'\right)^2 + E_2 p'' \tag{14}$$

Here $p = p(\eta)$, $S = S(\eta)$ and the superscripts $'$ and $''$ are used to represent the first and second derivatives with respect to η.

The core is assumed to be initially saturated with liquid water and at some pressure $p = p_{initial}$. At time $t = 0$, the pressure at one end of the core (denoted x=0) is reduced to $p = p_{final}$. Therefore, at $t = 0$ or as x tends to infinity (both equivalent to η tending to infinity), we have $S = 1$, $p = p_{initial}$, and $p' = 0$. At $x = 0$ or as t tends to infinity (equivalent to $\eta = 0$), $S = S_{final}$, $p = p_{final}$, and $p' = p'_{final}$. S_{final} and p'_{final} are unknown, but may be determined using standard numerical techniques.

Under these boundary conditions, Equations (13) and (14) can be solved numerically to obtain liquid saturation and pressure distributions along the porous medium sample, providing a description of the progression of the boiling front as it moves through the porous medium.

2.2 Separable Phase (SP) Flow Model

In the case of separable phase flow, a two-phase Darcy Law is used in determining the mass flow rate per unit area. The fluid mass and energy per unit volume of formation, and the mass and energy fluxes per unit area in this case are given by

$$A_m = \phi\left[S\rho_l + (1-S)\rho_g\right] \tag{15}$$

$$A_e = (1-\phi)\rho_r c_r T_{sat} + \phi\left[S\rho_l u_l + (1-S)\rho_g u_g\right] \tag{16}$$

$$\mathbf{Q}_m = k\left(k_{rl}\frac{\rho_l}{\mu_l} + k_{rg}\frac{\rho_g}{\mu_g}\right)\left(-\frac{\partial p}{\partial x}\right) \tag{17}$$

$$\mathbf{Q}_e = k\left(k_{rl}h_l\frac{\rho_l}{\mu_l} + k_{rg}h_g\frac{\rho_g}{\mu_g}\right)\left(-\frac{\partial p}{\partial x}\right) + K\left(-\frac{\partial T_{sat}}{\partial x}\right) \tag{18}$$

In a similar manner to the solution of the HM flow case, the conservation of mass and energy equations given in (1) and (2) can be combined with Equations (15)-(18) and re-written in the form of Equations (11) and (12). In this case the coefficients A_1, A_2, B_1, B_2, C_1, C_2, D_1, D_2, E_1, and E_2 are again non-linear functions of pressure and saturation, but they are different from those used in the homogeneous mixture case. The similarity variable $\eta = x/\sqrt{t}$ is again used to write the conservation of mass and energy equations in the form of (13) and (14) and these equations are then solved numerically using the same boundary conditions given in Section 2.1.

2.3 Comparison of HM and SP Models

A comparison of calculated solutions for the homogeneous mixture flow model with those for the separable phase flow model shows that for a given pressure reduction at one end of a porous medium sample, more liquid water is predicted to be converted to gas in the HM case than in the SP case. It is also predicted that the boiling front progresses at a faster rate in the SP case than in the HM case.

This is illustrated in the following example. Consider a porous medium sample with $\phi = 0.18$, $k = 10^{-10}\text{m}^2$, $c_r = 1000$ J/kgK, $K = 2$ W/mK and $\rho_r = 2650$ kg/m^3. Assume that the sample is initially at a pressure $p_{initial} = 1.1$ bar; the pressure at one end of the sample is suddenly reduced to $p_{final} = 1$ bar. In the HM case, once the boiling front has completely moved through a particular part of the core, 95% of the liquid water in that area has been converted to water vapour ($S_{final} = 0.05$). In the SP case only 58% is converted ($S_{final} = 0.42$). It can also be shown that in the HM case it would take about 22 seconds for the boiling front to progress through 1 m of the core, while in the SP case it would take about 12 seconds to travel this same distance. Saturation and pressure distributions for the two cases are shown in Figure 3. (These distributions are plotted versus η. When plotted against the distance $x = \eta\sqrt{t}$ along the core, the curves are similar in shape but stretch out as time t elapses since depressurisation of one end of the core.)

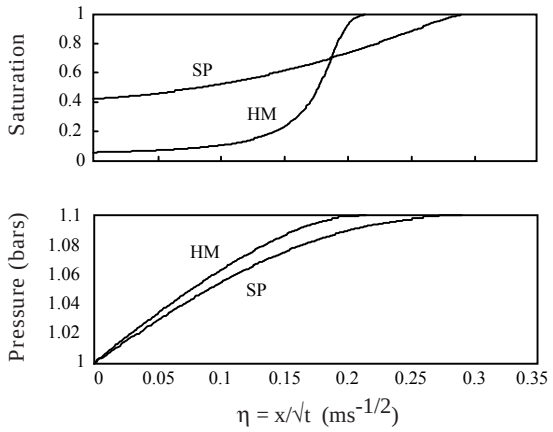

Figure 3. Saturation and pressure distributions in a one-dimensional horizontal porous medium sample.

3. PHYSICAL EXPERIMENT

This section reports on a physical experiment on rapid transient boiling in porous media, intended to provide data to be used to test the validity or otherwise of the mathematical models described in Section 2.

In this physical experiment, a porous medium sample is placed inside a containment vessel. The sample is then saturated with liquid water. A decrease in pressure at one end of the sample allows boiling to occur. A boiling front is initiated at the end of the vessel and quickly moves through the sample (see Figure 2). Nuclear Magnetic Resonance techniques are used to image the liquid water content throughout the sample over time, providing a picture of the progression of the boiling front as it moves through the core.

3.1 Apparatus and Procedure

The experimental apparatus consists of a containment vessel, connection hose, ambient condition reservoir, Nuclear Magnetic Resonance (NMR) equipment and a vacuum pump (see Figure 4).

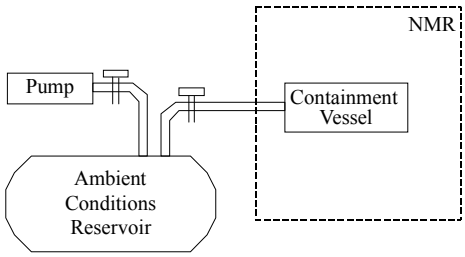

Figure 4. Experimental apparatus.

In the experiment, a cylindrical rock core was sealed around its sides and one end. Its other end remained open to allow the eventual flow of fluid from the rock to the ambient condition reservoir. The core was initially saturated with deionised water and its dimensions, average porosity, permeability and density were calculated.

A cylindrical brass chamber, 3 litres in volume, was used to provide "ambient" conditions for the experiment. Most of the air was removed from the reservoir enabling the pressure within the reservoir to be controlled by the temperature. [An addition of a small amount of water into the reservoir would then provide an ambient pressure of $p_{air} + p_{sat}(T_{ambient})$.] The temperature of the reservoir was reduced to $T_{ambient}$, a temperature low enough to provide ambient pressure conditions which would initiate boiling in the core.

A connecting hose of diameter 8 mm and length 2.5 m was filled with cold water. One end of the hose was connected to a closed tap on the ambient condition reservoir. The other end was connected to the core and the core was placed inside the NMR.

Once the experimental setup was in place and the NMR equipment ready, the vacuum pump was turned off and the initial pressure p_{air} and temperature $T_{ambient}$ inside the reservoir were recorded.

The experiment was initiated by opening the tap between the reservoir and the connecting hose. The cold water inside the hose boiled due to the pressure reduction and flowed into the ambient condition reservoir. The addition of this water to the reservoir provided the ambient pressure for the experiment of $p_{air} + p_{sat}(T_{ambient})$.

Shortly after the opening of the tap, boiling was initiated at the depressurised end of the core and the NMR equipment was used to measure the spatially distributed image of water concentration in the core.

3.2 Results

A number of laboratory experiments were performed using a bentheimer rock core of length 12.5 cm and diameter 3.8 cm. Approximate rock properties were: ρ_r = 2000 kg/m^3, $\phi = 0.18$, $K = 2$ W/mK, $c_r = 1000$ J/kg, and $k = 10^{-12}$ m^2. The initial temperature and pressure inside the ambient condition reservoir were $T_{ambient} = 2°$ C and $p_{air} = 5$ mbar providing an ambient pressure for the experiments of approximately $p_{air} + p_{sat}(T_{ambient}) = 12$ mbar.

Using NMR imaging, one-dimensional liquid saturation distributions along the core were found. Some NMR images are reproduced here with comments.

Experiment A: The core was initially at atmospheric conditions (approximately 1 bar and 20°C) and saturation distributions were found every 200 milliseconds for 25 seconds. Two measured saturation distributions are shown in Figure 5.

We have assumed the core was initially saturated with liquid water. An image of liquid saturation was taken before boiling was initiated and subsequent images have been normalised with respect to this initial distribution.

While data obtained shows a boiling front moving through the core as expected, the progression of the front occurs quickly and not enough information about the process is obtained. In less than 200 milliseconds [see Figure 5 (a)] boiling has apparently begun in the first 7 cm of the core, while in fewer than 400 milliseconds [see Figure 5(b)] boiling is occurring throughout the core. According to numerical results, this process should occur at a much slower rate.

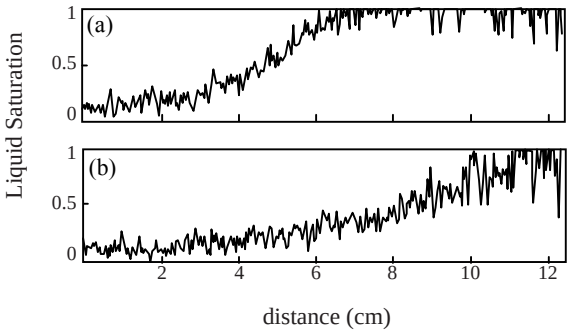

Figure 5. Experiment A. Two images of liquid saturation: image (a) was taken within 200 milliseconds of the onset of boiling, and image (b) a further 200 milliseconds later.

Experiment B: The core was again initially at atmospheric conditions. Saturation images in this case were found every half-second for 10 minutes. Three saturation distributions obtained are shown in Figure 6. Again, distributions have been normalised with respect to an initial scan.

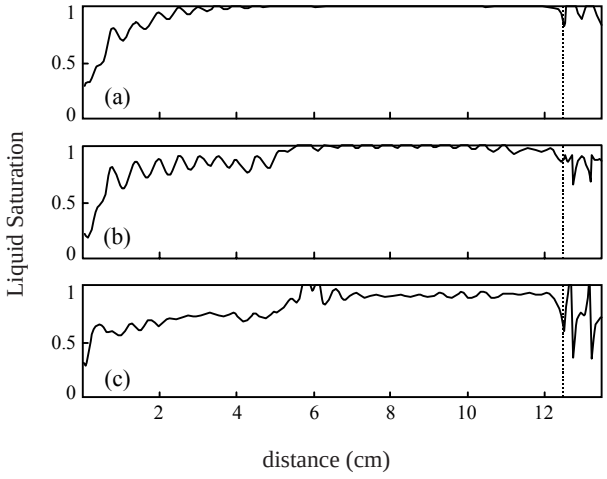

Figure 6. Experiment B. Three (normalised) images of liquid saturation: image (a) was taken within 0.5 sec of initiation of boiling, image (b) 0.5 seconds later, and image (c) approximately 8 minutes later.

Figure 6 (a) shows the initiation of a boiling front from the depressurised end. Boiling appears to also have begun at the closed end of the core even before the boiling front reaches this end. A small amount of water lies between the rock and the plastic endcap at this closed end. It is this "end water" which appears to begin to boil almost immediately (see portion of scan to the right of dotted line in Figure 6). The semi-infinite numerical solution does not model this phenomenon. In Figure 6 (b) the progression of the boiling front can be seen as well as the continuation of boiling in the water at the end of the core. Over time, some boiling occurs throughout the core [see Figure 6 (c)].

Further observations (not shown here) indicate increases in saturation at some regions at later times. Such an increase may be due to recondensation of moving steam. Upon removal of the core from the NMR, it was noted that the core felt cold to the touch. A qualitative deduction, then, is that the core was too cold for further boiling to take place under the conditions of the experiment.

The speed at which the boiling front moves through the core in Experiment B is closer to numerical estimates, but because the core is finite, the predictions of the semi-infinite model may not apply.

After Experiment A, the NMR was recalibrated to focus on smaller pore sizes. Hence, direct comparisons of front travel times in experiments A and B cannot be made.

4. COMPUTER SIMULATIONS

Several simulations using HYDROTHERM (Hayba & Ingebritsen, 1994) were carried out for comparison with both the finite core experiments and similarity solutions (SP flow only). Unfortunately pressures are constrained in HYDROTHERM to be no less than 0.5 bar so comparisons with the physical experiments are qualitative only.

Simulations were carried out for a one-dimensional core of length 14.5 cm, ρ_r = 2000 kg/m^3, ϕ = 0.18 , K = 2 W/mK, c_r = 1000 J/kg, and $k = 10^{-12}$ m^2. The core was assumed to be initially saturated with liquid water, at a pressure $p_{initial}$ = 1.1 bar and temperature $T = T_{sat}(p)$ = 102.3°C. Constant temperature and pressure conditions of pressure p = 1 bar and $T = T_{sat}(p)$ = 99.6°C were placed on the depressurised end.

When no-flow boundary conditions were placed on the end opposite that which was depressurised, a boiling front was initiated at the depressurised end and progressed through the porous medium [see Figure 7(a)]. As the system approached thermodynamic equilibrium, increases in liquid saturation were seen [see Figure 7(b)]. Calculated velocities indicated that water was flowing back into the core replenishing the depleted zone. Such late-time increases in liquid saturation indicate consistency in this aspect of the simulations and physical experiments. In the physical experiment this had a cooling effect on the region. In the event that such an effect were produced in hydrothermal eruptions, it would slow the eruption in progress, and any cooling effect on the area may explain long recovery times between subsequent eruptions.

When “end-water” was placed at the closed end of the porous medium, small scale boiling was indicated almost immediately in this water (not shown). This boiling, however, occurred in very small quantities in the simulations, much smaller than the NMR profiles indicated.

Good agreement between the simulation and the similarity solution was obtained up to the time at which the boiling front had progressed completely through the core. Late-time saturation increases are a feature of the finiteness of the core and are therefore not predicted by the similarity solution.

When constant temperature and pressure boundary conditions were placed on the end opposite that which was depressurised, we again saw the progression of a boiling front through the porous medium [see Figure 8(a)]. As this boiling front moves through the core, heat was removed from the system. Once the boiling front had progressed completely through the porous medium, increases in liquid saturation were again seen, but water velocities indicate in this case these were due to water being fed from the end opposite that which was depressurised. A liquid-resaturation front moved back through the core until the system eventually reached a steady state [see

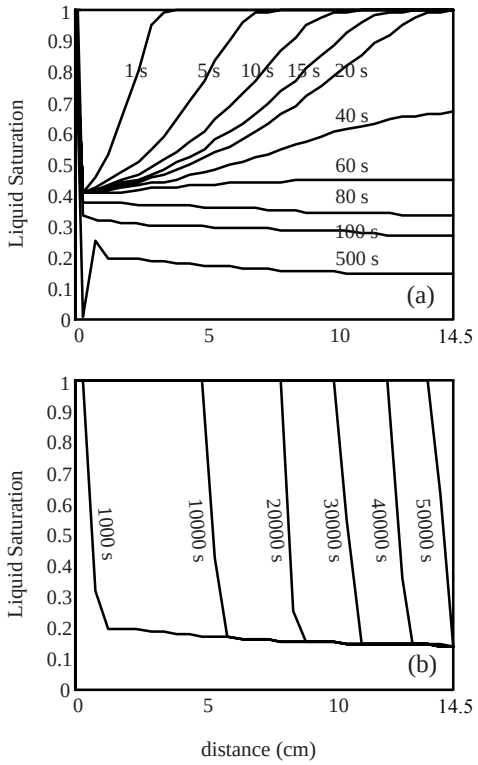

Figure 7. Saturation curves for one-dimensional core. Constant pressure and temperature conditions at x=0 cm, no-flow boundary conditions at x=14.5 cm. (See text for details.)

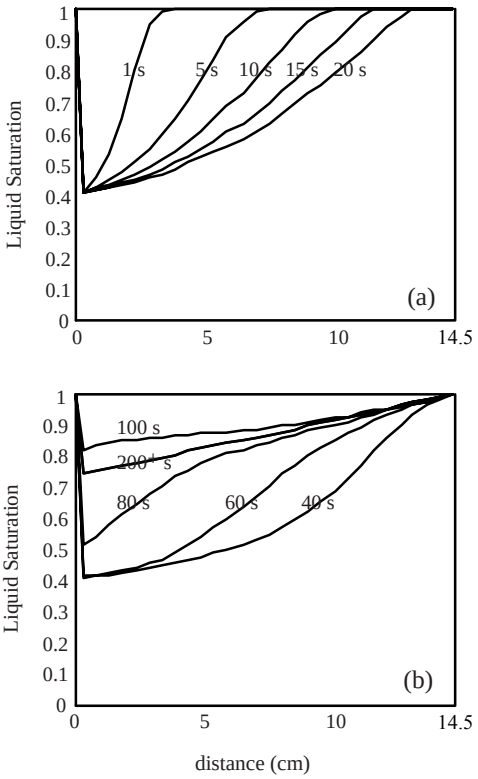

Figure 8. Saturation curves for one-dimensional core. Constant pressure and temperature conditions at both ends. (See text for details.)

Figure 8(b)]. Comparisons in this case cannot be made with the NMR experiment as the physical experimental system was closed at one end.

Good agreement between the simulation and the similarity solution was again obtained up to the time at which the boiling front had progressed completely through the core.

5. SUMMARY AND CONCLUSIONS

Numerical and physical experiments were conducted to investigate some aspects of transient boiling processes in porous media. A one-dimensional semi-infinite mathematical model was solved and results compared with physical experimental data. Because physical experiments were constrained to be finite, direct comparison of all aspects of results was not possible. Both numerical and physical experiments show a boiling front initiated at one end of the porous medium. However, the rate at which the front progresses through the core and boiling effects at the closed end of the core appear to be features of the finiteness of the physical experiment which were not predicted by the semi-infinite model.

Both experimental and mathematical models are being modified in order to achieve consistency. It is hoped that improved models of this transient boiling process will further help the understanding of the physical mechanisms which drive hydrothermal eruptions.

ACKNOWLEDGEMENTS

The physical experiment detailed in Section 3 was done with funds provided by the Massey University Graduate Research Fund, the contribution of which is gratefully appreciated. Thanks are also due to Sarah Codd for her assistance with the NMR experiments and interpretation.

REFERENCES

Allis, R.A. (1984). *The 9 April 1983 Steam Eruption at Craters of the Moon Thermal Area, Wairakei*. DSIR Geophysics Division Report No. 196.

Bixley, P.F. and Browne, P.R.L. (1988). Hydrothermal eruption potential in geothermal development. *Proc. 10th NZ Geothermal Workshop 1988*, University of Auckland, 195-198.

Hayba, D.O. and Ingebritsen, S.E. (1994). The Computer Model HYDROTHERM, *A Three-Dimensional Finite-Difference Model to Simulate Ground-Water Flow and Heat Transport in the Temperature Range of 0 to 1,200°C.* U.S. Geological Survey Water-Resources Investigations Report 94-4045, 85p.

Muffler, L.J.P., White, D.E. and Truesdell, A.H. (1971). Hydrothermal explosion craters in Yellowstone National Park. *Geol. Soc. Amer. Bull.*, Vol. 82, 723-740.

Smith, T.A. and McKibbin, R. (1997). Modelling of hydrothermal eruptions: A review. *Proc. 19th NZ Geothermal Workshop 1997,* University of Auckland, pp.123-128.

Smith, T.A. and McKibbin, R. (1998). Towards a hydrothermal eruption flow model. *Proc. 20th NZ Geothermal Workshop 1998,* University of Auckland, pp.387-392.